Phonon-wind-driven transport of photoexcited carriers in a semiconductor quantum well

L. M. Smith, J. S. Preston, and J. P. Wolfe
Department of Physics and Materials Research Laboratory, University of Illinois at Urbana-Champaign, Urbana, Illinois 61801

D. R. Wake
Materials Research Laboratory, University of Illinois at Urbana-Champaign, Urbana, Illinois 61801

J. Klem, T. Henderson, and H. Morkoç
Coordinated Science Laboratory, University of Illinois at Urbana-Champaign, Urbana, Illinois 61801-3082
(Received 15 September 1988)

The in-plane transport of photoexcited carriers in $GaAsAl_{0.3}Ga_{0.7}As$ multiple quantum wells is measured optically with 10 ps and 4 μm resolution. The local carrier density is measured by the bleaching of the excitonic absorption line. The expansion of the photoexcited carriers following a 6-ps pump pulse is found to be a strong function of excitation power and ambient temperature. At low powers, with initial carrier densities $n_0 \leq 2\times10^{11}$ cm^{-2}, the spatial distribution is well described by a single expanding Gaussian profile corresponding to an effective diffusion constant $D_{\rm eff}(n_0,T)$. The power and temperature dependence suggests a phonon-wind driving mechanism. At higher densities ($n_0 > 2\times10^{11}$ cm^{-2}) a narrow spatial profile appears which we attribute to "thermal confinement" of carriers within a phonon hot spot. After some delay, the "confined"-carrier distribution is observed to undergo a rapid expansion. This unusual effect is attributed to the "explosion" of the phonon hot spot, as predicted by Kazakovtsev and Levinson.

INTRODUCTION

A wealth of intriguing physics has been uncovered through the study of $GaAs/Ga_xAl_{1-x}As$ quantum wells and superlattices. In this system, free electrons and holes both migrate to the lower-band-gap GaAs regions.[1] If the layer thickness is not too thin, the electronic states in these structures are those of free particles confined in one dimension to a simple square-well potential.[2] The resulting confinement perpendicular to the layers leads to a series of conduction and valence subbands with spacings determined by the depth and width of the quantum well.

The confinement of the carriers results in many properties which are of both fundamental and technological interest. An example is the use of modulation doping techniques[3] which spatially separates the donor/acceptor ions from the carriers. This not only leads to exceptionally high mobilities, but also allows weaker scattering mechanisms such as interface roughness[4] to be studied. A number of studies have examined the carrier mobility in both n- and p-type material. It is typically found that the conduction electrons have mobilities on the order of 10^6 cm^2/V s at 4 K.[5] The mobility for p-type material is much less,[6] as expected due to the higher mass of the hole. The confinement also influences the optical properties, in part through an enhancement of the exciton binding energy. This leads to an exciton absorption resonance which is observable up to room temperature,[7] but which can be easily saturated by photoexcited carriers. A number of novel optoelectronic devices have been proposed based on this optical nonlinearity.[8] We note that the ultimate performance to be expected from such nonlinear optical devices will depend upon the transport properties of the photoexcited carriers.

In our present experiments we have studied the lateral motion of photoexcited carriers in GaAs quantum wells, using the decrease in an exciton absorption line as a measure of the local carrier density. Recently, several attempts have been made to measure the lateral transport of photoexcited carriers by other means. Hegarty and Sturge[9] used a transient-grating technique with near-resonant excitation of excitons and obtained diffusion constants at 5 K for the excitons that ranged from 0 to 20 cm^2/s depending on the excitation wavelength. At the opposite extreme, using time-resolved Raman scattering at 10 K, Tsen and Morkoç[10] concluded that the carriers had an extremely high drift velocity of 8×10^6 cm/s. Finally, Hillmer, Forchel, Hansmann, Lopez, and Weimann[11] used a photoluminescence time-of-flight technique and obtained ambipolar diffusion constants of approximately 65 cm^2/s at $T=98$ K. The differences between these earlier results motivated us to attempt to more directly determine the time-resolved carrier spatial distributions by imaging the absorption following photoexcitation with a short pump pulse. We are able to achieve the necessary temporal and spatial resolution by measuring the absorption of a weak probe pulse tuned to the exciton resonance as a function of position and time delay.

Our results indicate that in some cases the carrier distributions are nearly stationary, but under other circumstances the carriers are indeed mobile, propagating with near-sonic velocities. Presumably the less mobile holes will dominate the ambipolar transport of the pho-

toexcited carriers so that our results might be expected to coincide with the electrical measurements of p-type material. However, we find that the temperature and density dependence of the transport of photoexcited carriers is much more complex than in the modulation doping case.[6] This is due to the nonequilibrium nature of the carriers and phonons produced in the photoexcitation region. The interpretation of the transport for the photoexcited case requires a careful consideration of the coupling of the carriers to the lattice.

EXPERIMENTAL METHODS

In the absorption spectra of a GaAs multiple quantum well (MQW), several resonances are observed which arise from the direct generation of excitons. These resonances can be labeled according to the contributions of the conduction and valence subbands. In Fig. 1(a) an absorption spectrum recorded by Pearah *et al.*[12] is shown for one of our samples (30-layer $GaAs/Al_{0.3}Ga_{0.7}As$ with 210-Å GaAs wells). The various resonances are labeled according to the subband quantum numbers. The slightly

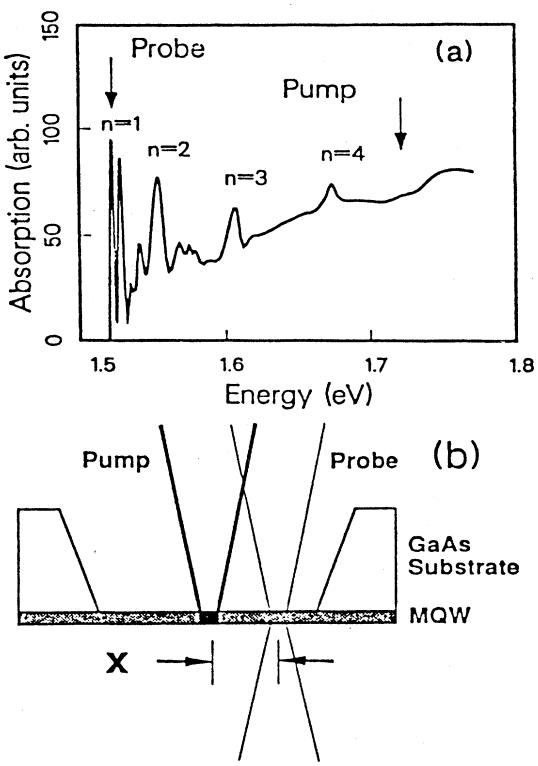

FIG. 1. (a) Absorption spectrum of a 30-layer MQW comprised of 210-Å GaAs wells and 100-Å $Al_{0.3}Ga_{0.7}As$ barriers. This data was taken from Ref. 12, and corresponds to the same crystal used in our experiments. Allowed excitonic optical transitions are labeled by their principal quantum number. The position of pump and probe photon energies are shown by the arrows. (b) Drawing of the sample showing the 1-mm region where the substrate is removed. The probe beam is scanned relative to the pump beam in order to obtain the spatial distribution of nonequilibrium carriers produced by the pump beam.

different confinement and binding energies of excitons composed of light and heavy holes produce the doublet observed at the lowest energy. The $n=1$ heavy-hole exciton absorption line occurs at lowest energy and has the strongest oscillator strength.

In our experiments, we measure the change in the optical absorption at the heavy-hole exciton resonance due to the presence of photoexcited carriers. It has previously been demonstrated that the strength of the absorption line is reduced (bleached) in the presence of nonequilibrium carriers.[13,14] This bleaching occurs in part from Coulomb screening by the carriers, and in part from filling the electronic states in the two-dimensional (2D) bands from which the excitons are created.[15,16]

We employ two dye lasers, synchronously pumped by an actively mode-locked Ar^+ laser, for the pump and probe beams. The experimental arrangement is summarized in Fig. 2. The pump laser, operating with Pyridine 2 as the organic dye, has a temporal width of 6 ps or less. The probe laser uses Styryl-8 as the active medium and has a temporal width of approximately 6 ps. The probe wavelength is tuned using a three-plate birefringent filter. As shown in Fig. 1(a) the weak probe is tuned resonantly to the $n=1$ heavy-hole exciton line while the pump beam is operated at 1.72 eV (720 nm), which is approximately 4 LO-phonon energies above the $n=1$ band edge. The two dye-laser pulses are delayed relative to each other by variable delay lines. Each beam is independently focused externally and the two focal spots are then imaged onto

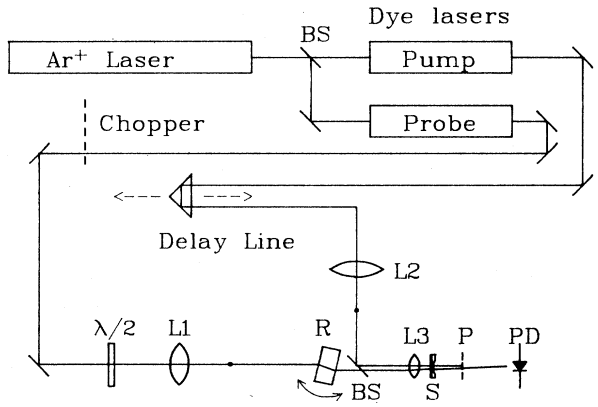

FIG. 2. Diagram of the experimental apparatus for picosecond absorption imaging. A mode-locked Ar^+ laser pumps both the pump and probe dye lasers. In the configuration shown, the probe beam is chopped for phase-sensitive detection and its polarization is rotated by a half-wave plate, $\lambda/2$, prior to being focused by the external lens, L1. The pump beam undergoes a variable delay before being focused by the external lens L2. The focal points of L1 and L2 are shown schematically in the diagram as dots in the beam paths. The probe beam's relative position is controlled by its refraction through a rotatable transparent block R. The two beams are recombined by a polarizing beam splitter BS before their external foci are imaged onto the sample S by the microscope objective L3. Finally, the transmitted probe beam passes through a polarizer P to be detected at the Si p-i-n photodiode PD.

the sample by an 11-mm–focal-length microscope objective mounted on the sample probe. The best focus obtained for each beam is approximately 3 μm, yielding an ultimate spatial resolution of ~ 4 μm (the convolution of the pump and probe laser spots). Typical temporal resolution of the system, as given by the cross correlation of the pump and probe pulses, is less than 10 ps. The spectral resolution of absorption spectra is limited by the spectral width of the probe beam to be ~ 4 Å.

Both the pump and probe beams are linearly polarized and are adjusted to be orthogonal by a half-wave plate in the pump-beam path. The probe beam can be scanned across the sample by refraction through a rotatable lucite block. The beams are then recombined with a polarizing beam splitter before being focused onto the sample. The light transmitted through the sample is collected and collimated before passing through a polarizer to the *p-i-n* avalanche photodiode detector. The polarizer prevents the portion of the pump beam transmitted by the sample from reaching the detector. Phase sensitive detection is used to improve the signal-to-noise ratio; however, the choice of chopping the pump or probe beams depends on the type of measurement being made.

Two distinct types of measurements are found to be particularly useful in characterizing the carrier transport. The first of these involves fixing the spatial position of the two beams and taking absorption spectra as a function of the temporal delay. In the second type of experiment the probe wavelength is fixed to the peak of the heavy-hole exciton resonance and is spatially scanned relative to the pump-laser spot, as shown in Fig. 1(b). Typically, the probe beam is chopped to take absorption spectra, resulting in a signal that is proportional to the absolute transmission of the probe beam. However, during spatial scans the pump beam is usually chopped so that only the relative transmission of the probe beam is measured. Since this chopping scheme eliminates the uniform background from the transmitted probe beam, its sensitivity is significantly higher.

In the following section, typical time-resolved spectral and spatial data will be described for two multiple quantum wells with different well widths (210 and 290 Å). Both samples consist of 30 wells of GaAs separated by 100-Å barriers of $Al_xGa_{1-x}As$ ($x=0.3$). The use of multiple wells increases the sensitivity of the experiment, since each GaAs layer absorbs only a small fraction of the incident beam. The excitation in the different quantum wells is reasonably uniform since the total thickness of the MQW is slightly less than 1 absorption length at the pump wavelength. As shown in Fig. 1(b) the substrate has been etched off leaving only the layered material. This is necessary because the GaAs substrate would strongly absorb the laser beams. The MQW side of each sample is glued to a glass microscope cover slip before the portion of substrate is etched away. Repeated thermal cycling of the samples produced local inhomogeneities in the exciton absorption which we attribute to thermal stresses. For this reason detailed comparisons between the two samples is not performed. However, where measurements overlapped qualitatively similar results were obtained for both samples.

EXPERIMENTAL RESULTS

Examples of time-resolved absorption spectra for a 210-Å GaAs multiple quantum wells (MQW) at 8.5 K, with the pump and probe spatially overlapped are shown in Fig. 3(a). The spectra clearly show the bleaching associated with the production of carriers by the pump beam. The full width at half maximum of the pump pulse is 3 μm. The average areal density of the photoexcited carriers can be estimated from the incident photon flux, the measured absorption coefficient of the MQW (Ref. 12) and the assumption of equal carrier population in the wells. In this case, we estimate an initial density of 1×10^{11} cm^{-2} per well.

In addition to the bleaching effect, a small shift can also be observed in the position of the transmission dip. Using the known temperature dependence of the energy position of the exciton resonance,[17] the average lattice temperature of the probed area can be determined as a function of time. The results are shown in Fig. 3(b), where an exponential decay has been fitted to the results. If the phonon propagation is ballistic at 8.5 K, the time required for the excess phonons to escape the photoexcited region is approximately given by the spot radius divided by the sound velocity. In our case the spot radius is

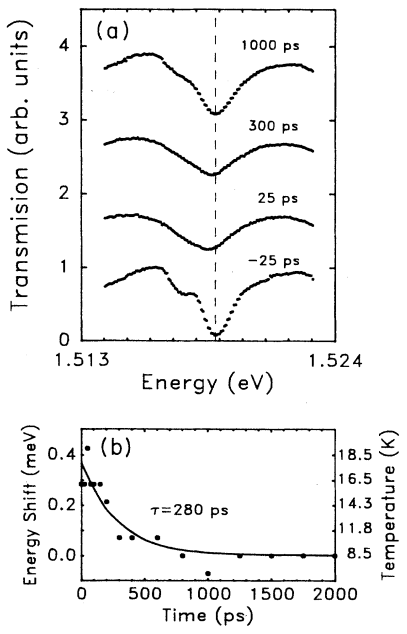

FIG. 3. (a) Time-resolved probe transmissions spectra for the 210-Å GaAs MQW at 8.5 K obtained by varying the probe wavelength (energy). The initial photoexcited-carrier density is 10^{11} cm^{-2} as determined from the incident energy and the measured absorption of the MQW. The $n=1$ heavy-hole exciton transmission dip is reduced by the presence of the nonequilibrium carriers produced by the pump beam at $t=0$ ps. The spectra are vertically displaced for clarity. (b) The shift in the position of the transmission dip as a function of time. The scale to the right shows a conversion to the equivalent lattice temperature, using the known band-gap shift with temperature (Ref. 17). An exponential decay has been fitted to the data.

1.5 μm, while the sound velocity in GaAs is roughly 5000 m/s, leading to a thermal relaxation rate of roughly 300 ps. This agrees quite well with the measured 280-ps cooling time.

Spatial scans of the probe-beam transmission are shown in Fig. 4 for initial carrier densities of 3×10^{10} cm^{-2} and 1×10^{11} cm^{-2}. The dots shown represent the local change in transmission. Note that the heights of the distributions have been normalized. At these excitation levels the spatial profiles can be well described by Gaussian line shapes as shown by the solid curves in the figure. While for both excitation levels significant expansion occurs in the first 1000 ps, the carriers clearly migrate much farther at the higher excitation level. This strong power dependence is not expected for a simple diffusion of particles.

In Fig. 5 we analyze the expansions shown in Fig. 4 in terms of a power-dependent diffusion constant. In the figure, the square of the full width at half maximum (Δ^2) is plotted as a function of delay. For carriers undergoing diffusive motion, the evolution of Δ^2 is given by $\Delta^2(t)=\Delta_0^2+16(\ln2)Dt$. The best fits to our data are given by diffusion constants of 73 and 24 cm^2/s for the high and low excitation levels, respectively.

One possible explanation of the power-dependent diffusivities is that the carriers are being driven away from the excitation region by a phonon wind. It is well known that the thermalization and recombination of the photoexcited carriers produces a significant source of nonequilibrium acoustic phonons. The result of localized excitation is a nonequilibrium phonon flux directed outward from the excited region. These directed phonons are continually absorbed by the carriers and then reemitted in random directions. This leads to a net transfer of momentum from the phonons to the carriers. This type of drift motion has been shown to be the dominant transport mechanism for electron-hole droplets (EHD) in Ge and Si.[18] The phonon-wind mechanism has also been invoked to explain excitonic transport in CdS.[19]

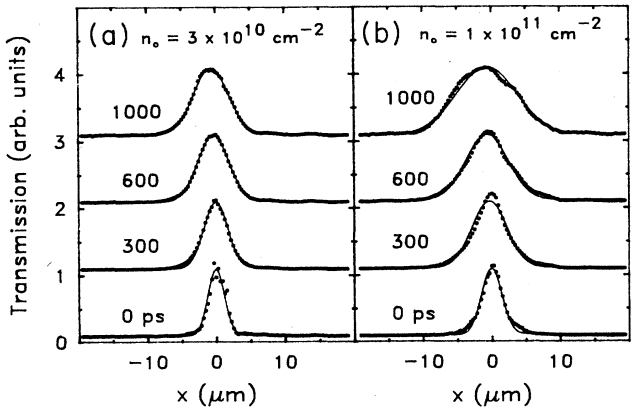

FIG. 4. Time-resolved spatial scans of the carrier distribution as a function of time after photoexcitation by a 6-ps pump pulse. Estimated initial carrier densities are (a) 3×10^{10} cm^{-2} and (b) 1×10^{11} cm^{-2}. The solid curves represent Gaussian fits to the data. The dependence of expansion rate on excitation power is not expected from simple particle diffusion. Data is for the 210-Å GaAs MQW.

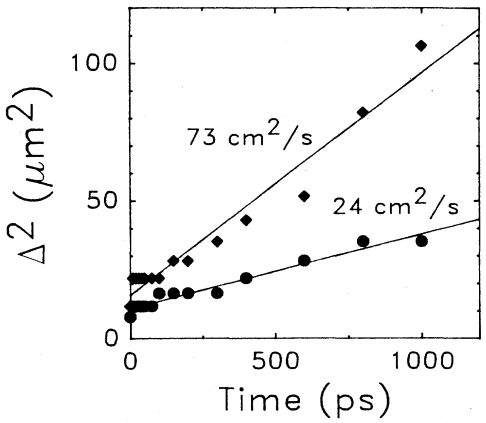

FIG. 5. Plot of Δ^2 as a function of delay time for the data shown in Fig. 4. The closed circles and diamonds correspond to initial densities of 3×10^{10} cm^{-2} and 1×10^{11} cm^{-2} respectively. The solid lines represent fits to the data, yielding the diffusion constants shown.

A simple expression for the phonon-wind force F on the carriers is given by

$$F=\gamma\mathcal{P}(1-v/v_s)\ , \tag{1}$$

where $\mathcal{P}$ is the phonon flux, γ is a coupling constant, and v and v_s are the local carrier drift velocity and the sound velocity, respectively. The factor $(1-v/v_s)$ expresses the fact that the phonons cannot push the carriers at drift velocities exceeding the sound velocity. The drift velocity is also related to the force by the expression

$$v=q\mu\mathcal{F}\ , \tag{2}$$

where μ is the particle mobility. (The charge q is included so that the mobility has the standard units for carrier drift in an electric field.) Equations (1) and (2) may be combined to give a carrier drift velocity in terms of μ, γ, $\mathcal{P}$, and v_s.

What form of expansion $\Delta(t)$ is expected for such a phonon-wind mechanism? Let us assume that in two dimensions the phonon flux at a radial distance ρ from a source of radius ρ_0 has the form $\mathcal{P}=\mathcal{P}_0(\rho_0/\rho)$, and that $v\ll v_s$. (We will consider $v\approx v_s$ below.) The position of a particle in this force field is given by integrating $\int_0^t dt=\int_{\rho_0}^{\rho}d\rho/v$. Using $v=q\mu\gamma\mathcal{P}_0\rho_0/\rho$ from Eqs. (1) and (2), we find

$$\rho^2(t)-\rho_0^2=2q\mu\gamma\rho_0\mathcal{P}_0t\ . \tag{3}$$

This result may be contrasted with the three-dimensional case where $r^3(t)-r_0^3\propto t$, which was experimentally verified for EHD in Ge by Greenstein and Wolfe.[20] Of course, the form of the spatial distribution depends upon the temporal distribution of the laser pulse but we can crudely identify ρ^2 with Δ^2. The result for 2D phonon-wind transport, $\Delta^2-\Delta_0^2\propto t$, is precisely the form expected for diffusive transport. Using the diffusion formula given above, we find an effective diffusion constant,

$D_{\text{eff}}=2q\mu\gamma\rho_0\mathcal{P}_0/16\ln 2$.

The analysis in terms of phonon-wind driving mechanisms shows that D_{eff} quite naturally depends on the excitation level through $\mathcal{P}_0$. Also, the observed power dependence of the expansion seems to argue against simple particle diffusion, where the scattering by phonons, defects, or impurity scattering is independent of density. Our experimental results show that the diffusivity increases with increasing particle density. Along those lines, Hegarty and Sturge[9] observed an increase in the diffusivity of resonantly produced excitons as their excess kinetic energy was increased. They suggested that the low-energy excitons were localized by fluctuations in the well potential. However, in our experiments, the excess energies are far above those used by Hegarty and Sturge and such localization is unlikely. Still, at this stage, we cannot completely exclude the possibility that defect or impurity scattering could depend on the density of photoexcited carriers.

To try and further distinguish between defect-limited diffusion and phonon-wind drift we have examined (1) the relation between v and excitation power and (2) the temperature dependence of D_{eff}. The dependence of average expansion velocity on pulse energy is shown in Fig. 6. The solid lines in Fig. 6(a) are least-squares fits to $\Delta(t)$ for the 290-Å GaAs MQW at 4 K. The resulting average velocities are plotted as the closed circles in Fig. 6(b). [Note that in Fig. 6(a), we plot Δ instead of Δ^2 as in Fig. 5. For these rather small fractional changes in Δ, it is not possible to distinguish between these functional dependencies for either data set.]

If we assume that the phonon-wind strength is proportional to the incident energy and that the damping is insensitive to the drift velocity, then it is straightforward to derive from Eqs. (1) and (2) an expression for the drift velocity of carriers v as a function of incident energy ε,

$$v/v_s=\alpha\varepsilon/(\alpha\varepsilon+v_s) \tag{4}$$

where $\alpha=q\mu\gamma\zeta$, with ζ defined as the ratio of the phonon flux at a given radius to the incident laser energy; i.e., $\mathcal{P}=\zeta\varepsilon$ by our initial assumption. Plotted in Fig. 6(b) is a curve of the form of Eq. (4), where α is the only fitting parameter. We have used an isotropic average for the longitudinal sound velocity in GaAs of 5100 m/s. The observed saturation behavior of v near v_s is precisely of the form expected for phonon-wind driven transport.

Important information can be obtained from the temperature dependence of the expansion. The temperature dependence of the effective diffusion constant for $n_0=1\times10^{11}$ cm^{-2} is shown in Fig. 7(c). The diffusion

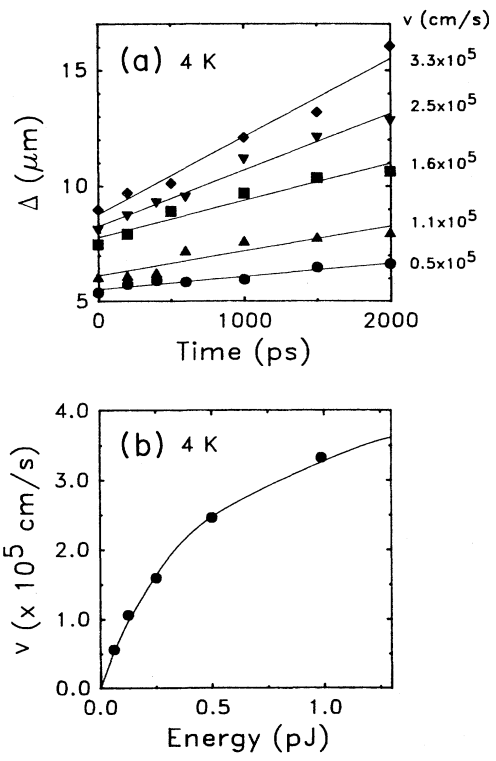

FIG. 6. (a) Plot of Δ vs time for pump energies of 0.06 (circles), 0.12 (triangles), 0.25 (squares), 0.5 (inverted triangles), and 1.0 pJ (diamonds) for the 290-Å MQW at 4 K. Straight lines are best fits to data, with slopes yielding the average expansion velocities of the distributions. (b) Plot of the above expansion velocities vs pump power. The solid curve is a fit to the data based on the presence of a phonon wind, as discussed in the text.

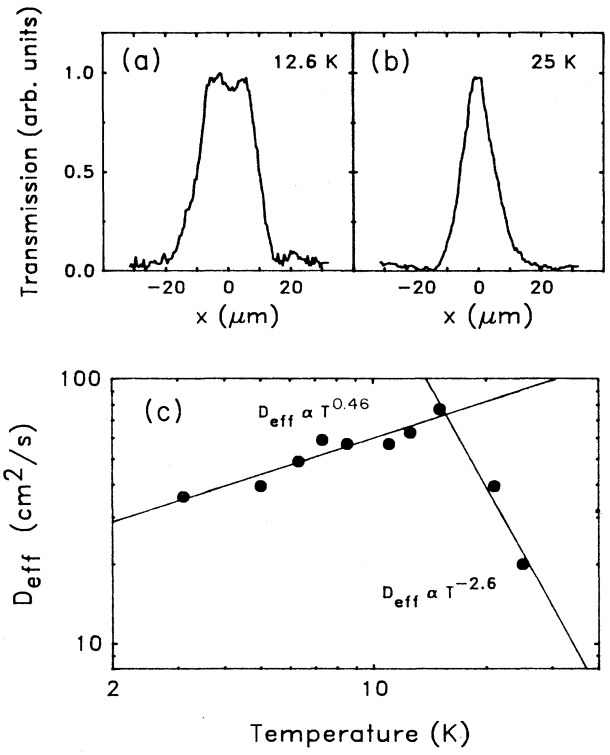

FIG. 7. Carrier expansion as a function of temperature at initial carrier densities of 10^{11} cm^{-2} (290-Å GaAs MQW sample). Spatial scans in (a) and (b) show the spatial distribution of the carriers 4 ns following the excitation pulse. The temperature dependence of experimentally determined effective diffusion constants is shown in (c). The effective diffusion constants plotted in this figure are fits to data taken after 1 ns to ensure that the carriers have thermalized with the lattice.

constants shown are obtained by fitting Δ^2 for delay times between 1 and 4 ns for the 210-Å GaAs MQW. This ensures that the carriers are thermally equilibrated with the lattice. At low temperatures, D_{eff} increases with temperature, roughly as $T^{1/2}$. The increase in D_{eff} with increasing temperature is not characteristic of the carrier-acoustic phonon-scattering mechanism in two dimensions, which predicts a temperature-independent diffusion constant.[21] However, it is consistent with a temperature-independent mean-free path determined by defect scattering. In this case, the diffusion constant scales with the thermal drift velocity as $T^{1/2}$.

For temperatures in excess of 15 K the effective diffusion coefficient sharply decreases with temperature. This effect is seen directly in the spatial profiles of Figs. 7(a) and 7(b). It is unlikely that we can relate the decrease in D_{eff} over this small temperature range to the onset of a new scattering process. Hole-mobility measurements[6] over this temperature range show no such precipitous drop in the mobility. On the other hand, a natural explanation for the sharp decrease in D_{eff} above 15 K is the thermal damping of the phonon wind by equilibrium phonons. At high enough ambient temperatures, the transport of the excess thermal energy away from the photoexcited region must be diffusive rather than ballistic and the strength of the phonon-wind force will decrease significantly. Specifically, the phonon wind should be greatly reduced when the ambient temperature is raised to the point where the phonon mean free path becomes comparable to the width of the initial carrier distribution. It is well known that the phonon mean free path decreases rapidly with increasing temperature due to Umklapp processes.

In order to determine whether this mechanism can account for the sharp drop in D_{eff} above 20 K, we must estimate the mean free path of the photons comprising the phonon wind. In general, this is a very difficult problem because the nonequilibrium frequency distribution is unknown. However, we can estimate the mean free path for a "typical" thermal phonon as a function of temperature. To estimate the thermal mean free path l, we note that the thermal conductivity κ is related to the specific heat C_V through $\kappa=\frac{1}{2}C_V v_s l$. The thermal mean free path can therefore be determined from known thermal conductivity[22] and specific-heat data.[23] The results are shown in Fig. 8 for two GaAs samples with different impurity concentrations.[22] Although our samples are undoped, we expect that the presence of the barrier layers and inhomogeneities in the interfaces will lead to an l closer to the more heavily doped case in Fig. 8. For the impurity level considered, the thermal mean free path decreases rapidly with temperature, and drops below 10 μm at a temperature of about 20 K. These estimates strongly suggest that the drop in D_{eff} at higher temperatures results from a sharp decrease in phonon-wind strength.

There are several reasons why the phonon wind could lose its effectiveness even below a bath temperature of 20 K. The presence of nonequilibrium phonons from the pump pulse tends to raise the local temperature above the bath temperature. Also, the strong frequency dependence of phonon-phonon scattering will cause the high-

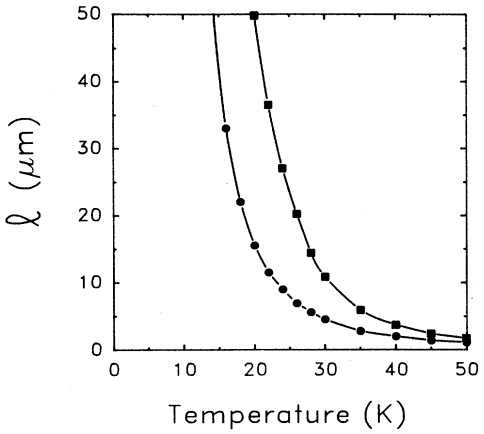

FIG. 8. Mean free path l associated with a Planck distribution of phonons as a function of temperature. The two plots correspond to impurity concentrations of 10^{16} cm^{-3} (squares) and 3×10^{18} cm^{-3} (circles), and were determined from the specific heat and thermal conductivity measurements in Refs. 22 and 23.

frequency nonequilibrium phonons comprising the phonon wind to have a shorter mean free path than the ambient thermal phonons. It will be seen shortly that the modification of the phonon wind due to local heating of

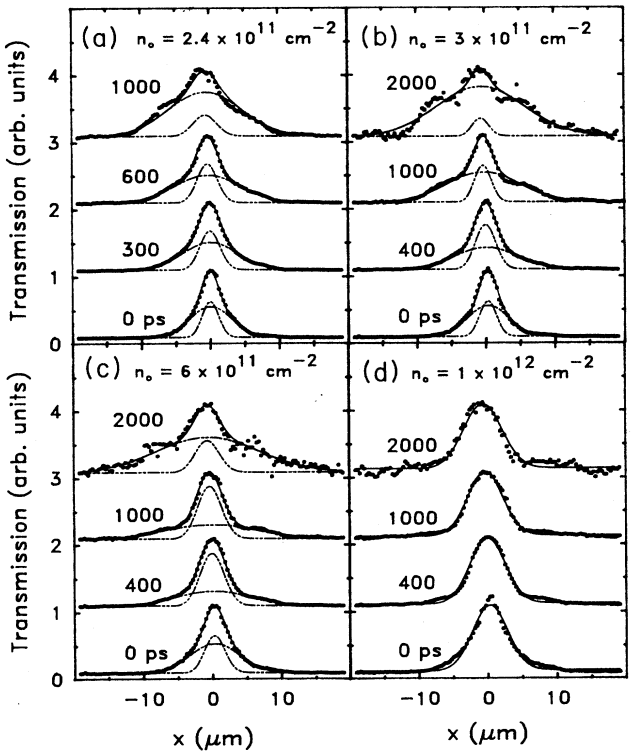

FIG. 9. Time-resolved spatial scans of carrier distributions after photoexcitation by pump pulse in the 210-Å MQW at 8.5 K. The initial carrier densities ar (a) 2.4×10^{11}, (b) 3×10^{11}, (c) 6×10^{11}, and (d) 1×10^{12} cm^{-1}. Solid lines are best fits to the data using either one or two Gaussian components. Those distributions with two components have each component displayed as dashed lines.

the lattice also plays an important role in the carrier expansion at lower ambient temperatures but higher excitation powers.

To summarize our results for low excitation powers ($n_0 \leq 10^{11}$ cm^{-2}), we observe carrier expansion velocities which strongly increase with carrier density. The power dependence of D_{eff} shows a saturation behavior at v_s characteristic of a phonon-wind mechanism. Furthermore, we find that the transport is strongly inhibited for ambient temperatures above 15 K. All of these results are consistent with the interpretation that the carriers have intrinsic diffusivities less than 20 cm^2/s but are driven away from the excitation region through the presence of a phonon wind.

We now examine what happens as the excitation level is increased further. In Fig. 9 the spatial expansions for initial carrier densities greater than 10^{11} cm^{-2} are shown. In striking contrast to the spatial distributions at lower powers, these spatial distributions cannot be fit by a single Gaussian component. A distinct new component appears which is narrower than the distributions associated with lower excitation levels. At these higher levels, the profiles are well characterized with by two Gaussian components as shown in Figs. 9(a)–9(c). As the pump energy increases, the relative contribution of the narrower component increases. At the highest excitation level, corresponding to $n_0 = 10^{12}$ cm^{-2}, the carrier distribution is well described by a single, slowly expanding Gaussian component as shown in Fig. 9(d). The analysis in terms of two independent Gaussian components provides two distinct effective diffusion rates, which are shown in Figs. 10(a)–10(c). In each case, the slowly expanding central component corresponds to an effective diffusion constant $\lesssim 5$ cm^2/s. The high-excitation data shown in Fig. 9(d) can be fitted with a single effective diffusion constant of 4 cm^2/s.

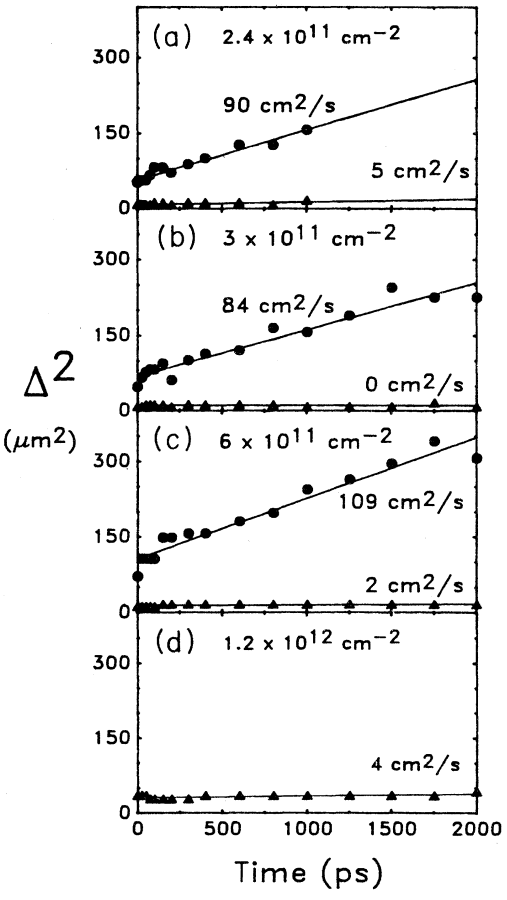

FIG. 10. Plot of Δ^2 from the fits shown in Fig. 9. Straight lines are best fits to the data, with slopes corresponding to the D_{eff}'s shown. Where two components are used to fit the spatial distributions of Fig. 9, Δ^2 for both components are plotted.

In Fig. 11 we summarize the effective diffusion constants observed in Figs. 5 and 10. At the lowest densities (region I), a single component with power-dependent diffusivity is observed. At intermediate densities (region II), a slowly diffusing component appears. At the highest densities (region III), the slowly diffusing component is dominant.

Can the slowly expanding component be attributed to a condensation of the carriers due to attractive many-body interactions? This component is observed up to the highest temperature used in the experiment, 35 K. We believe, therefore, that the narrow component is not due to the nucleation of an electron-hole liquid, which for GaAs is expected to have a critical temperature of approximately 8 K.[24]

The confined distribution may, however, be understood in terms of the thermally damped phonon-wind model that was discussed earlier. We have previously shown that the mean free path of ballistic phonons is inhibited for ambient temperatures in excess of 15 K. Further, the presence of a high density of nonequilibrium phonons leads to an increase in the local "temperature." Thus the slowly expanding component likely indicates the formation of a localized region of diffusive phonon transport, i.e., a hot spot.[25–27] Carriers within the hot spot do not

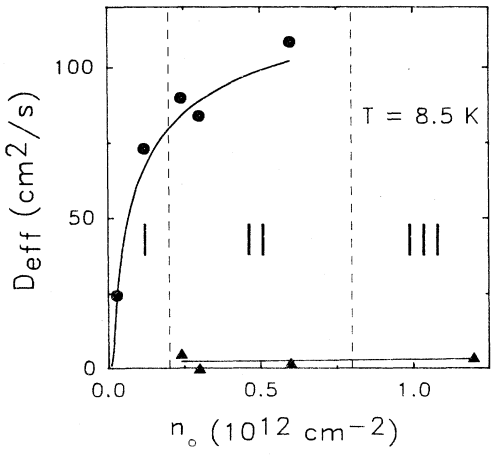

FIG. 11. Plot of D_{eff} as a function of excitation power in the 210-Å MQW at 8.5 K. Circles are data from the rapidly expanding components, while triangles represent the confined distributions observed at high powers. The graph has been separated into three regions based on whether the one- or two-component distributions are observed.

experience the net force associated with ballistic phonons, while carriers outside of this region are driven away by the ballistic phonons escaping from the surface of the hot spot. The width of the narrow component observed in the carrier distribution is therefore indicative of the spatial extent of the hot spot. In addition to feeling no phonon-wind driving force, carriers within the hot spot will have a tendency to be confined to the hot spot by the reduced band gap in the heated region.[28]

In order to determine if the creation of a localized hot spot is reasonable at the power levels used in our experiments, we estimate the effective temperature rise associated with the absorption of the optical pulse. The optical energy is initially absorbed within the electronic system. The hot photoexicted carriers then rapidly thermalize to an effective temperature through carrier-carrier collisions.[16,29] Subsequently, the hot carriers relax to the lattice temperature, first by rapid LO phonon emission, and then by slower acoustic phonon emission. The excess energy that is transferred to the lattice is eventually transformed into low-frequency acoustic phonons through anharmonic interactions. While the details of this highly nonequilibrium process are expected to be complex, we can define an effective local temperature through the specific heat and the local energy density in the lattice.

The results of this calculation as a function of incident energy is shown in Fig. 12. To facilitate comparisons with the spatial scans of the carrier distributions, the estimated density of carriers created is also given at the top of the figure. The two solid curves encompass the range of temperatures that are calculated depending on the amount of lattice heating arising from nonradiative recombination of the carriers. We can calibrate the calculation using the direct measurement of the local temperature as shown in Fig. 3. The result is the dashed line in Fig. 12, which corresponds to roughly 40% of the energy from the recombining carriers being deposited in the lattice.

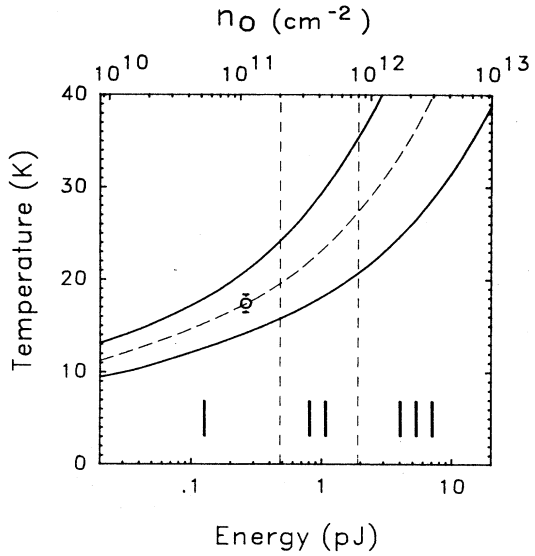

FIG. 12. Estimated maximum effective temperature attained as a function of the incident power absorbed per quantum well. The calculation was carried out for a 210-Å MQW with an initial temperature of 8.5 K. The two solid curves correspond to assuming that carrier recombination is nonradiative (upper curve) or radiative (lower curve). The dashed curve represent a radiative efficiency of 40% and fits the measured temperature rise shown in Fig. 3(b), as indicated by the open circle in this figure.

We are now in a position to compare the results of Figs. 11 and 12 in the three distinct excitation regimes. Region I corresponds to carrier distributions that are driven away from the excitation region by a ballistic phonon wind. The calculation in Fig. 12 indicates that the maximum lattice temperature attained remains below 20 K. It can be seen that the onset of the slow component in region II occurs for temperatures of about 20 K. As previously noted, at $\sim$20 K the mean free path for the phonons drops below 10 μm and the transport of the nonequilibrium phonons out of the excitation region will no longer be ballistic. In this region a hot spot is formed at the center of the excited spot so that carriers inside the hot spot are confined while carriers outside of the hot spot continue to be driven away. As a result, two distinct effective diffusion constants are observed in region II. Finally, in region III, the hot spot envelops almost all of the carriers so that only a very slow expansion is observed.

How does the hot spot evolve in time? The details remain to be examined; however, a striking manifestation of the hot spot is observed for delay times longer than 2 ns. In Fig. 13 the spatial expansion of carriers photoexcited at high excitation power is shown at several temperatures. At all temperatures, the confined component shows a slow expansion during the first 2 ns. For bath temperatures $\lesssim$25 K, this is followed by a rapid expansion. This can be understood in terms of the cooling of the hot spot. As the temperature associated with the hot

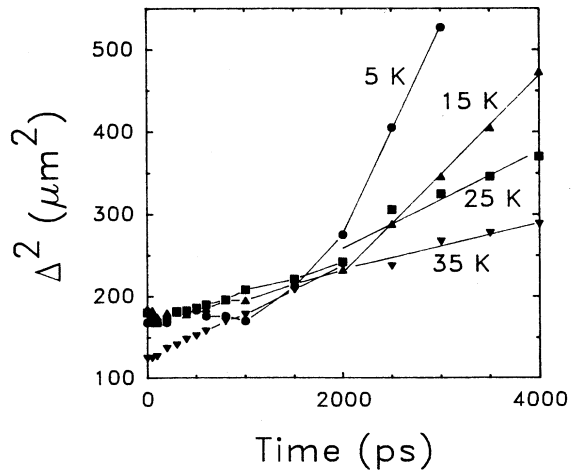

FIG. 13. Plot of Δ versus time over a 4-ns time span for an initial carrier density of 2×10^{12} cm^{-2}. Data was taken for the 210-Å MQW at 5, 15, 25, and 35 K. The knee at $t=2$ ns is interpreted as the explosion of the hot spot, which results in a strong ballistic phonon wind at $t>2$ ns, when $T\lesssim20$–25 K.

spot drops below 20 K, the phonon transport becomes ballistic and the hot spot "explodes." The terminology is that of Kazakovtsev and Levinson[30] who predicted just this type of behavior. The carriers still present after the hot spot explosion are then driven away from the excitation region by the resulting phonon wind. Note that at 35 K the carrier distribution expands slowly throughout the full 4.5 ns it is measured. This is expected since at this temperature, the transport of the phonons will be diffusive even in the absence of a hot spot.

CONCLUSIONS

In these experiments we have demonstrated a new technique to directly image the spatial distributions of photoexcited carriers in GaAs multiple quantum wells with 10-ps-temporal and 4-μm-spatial resolution. The results obtained on 210- and 290-Å quantum wells exhibit three distinctly different regimes of carrier transport, determined principally by the pump intensity. Our results at low densities indicate that the carriers have relatively low mobilities, presumably due to scattering from impurities and interface defects. The expansion rate of the carrier distribution following the 6-ps laser pulse, however, increases rapidly with pump power. The temperature and power dependence of the expansion indicates the presence of a driving force which we identify with a ballistic phonon wind.

At excitation powers above a critical threshold, the central portion of the carrier distribution remains nearly stationary. This can be attributed to the presence of a thermal hot spot. This conclusion is supported by a calculation of the lattice heating that is directly confirmed at lower powers. Once the hot spot has cooled below a critical temperature, it appears to explode, as predicted by Kazakovtsev and Levinson,[30] and we observe expansion at rates comparable to those observed at lower powers.

ACKNOWLEDGMENTS

This work was supported by U.S. Department of Energy Grant No. DE-AC02-76ER01198, by National Science Foundation (NSF) Grant No. NSF-DMR-85-21444, by University of Illinois Materials Research Laboratory Grant No. NSF-DMR-86-12680, and by the U.S. Air Force Office of Scientific Research. We are pleased to acknowledge the partial support from the National Science and Engineering Research Council of Canada for J.S.P. and from the Shell Companies Foundation and the IBM Corporation for L.M.S. Elements of the picosecond system were developed by D. Levi. We thank M. V. Klein for valuable advice and discussions.

[1]G. Duggan, J. Vac. Sci. Technol. B **3**, 1244 (1985).
[2]T. G. Gilbert and S. J. Gurman, Superlatt. Microstruct. **3**, 17 (1987).
[3]R. Dingle, H. L. Stormer, A. C. Gossard, and W. Wiegmann, Appl. Phys. Lett. **33**, 665 (1978).
[4]H. Sakaki, T. Noda, K. Hiradawa, M. Tanaka, and T. Matsusue, Appl. Phys. Lett. **51**, 1934 (1987).
[5]E. E. Mendez, P. J. Price, and M. Heiblum, Appl. Phys. Lett. **45**, 294 (1984).
[6]E. E. Mendez and W. I. Wang, Appl. Phys. Lett. **46**, 1159 (1985).
[7]D. S. Chemla and D. A. B. Miller, J. Opt. Soc. Am. B **2**, 1155 (1985).
[8]D. A. B. Miller, D. S. Chemla, T. C. Damen, A. C. Gossard, W. Wiegmann, T. H. Wood, and C. A. Burris, Phys. Rev. B **32**, 1043 (1985).
[9]J. Hegarty and M. D. Sturge, J. Opt. Soc. Am. B **2**, 1143 (1985).
[10]K. T. Tsen and H. Morkoç, Phys. Rev. B **34**, 6018 (1986).
[11]H. Hillmer, A. Forchel, S. Hansmann, E. Lopez, and G. Weimann, Solid State Electron. **31**, 485 (1988).
[12]P. J. Pearah, W. T. Masselink, T. Henderson, C. K. Peng, H. Morkoç, G. D. Sanders, and Yia-Chung Chang, J. Vac. Sci. Tech. B **4**, 525 (1986).
[13]J. Kash and J. Tsang, Phys. Rev. Lett. **54**, 2151 (1985).
[14]D. A. B. Miller, D. S. Chemla, D. J. Eilenberger, P. W. Smith, A. C. Gossard, and W. T. Tsang, Appl. Phys. Lett. **41**, 679 (1982).
[15]S. Schmitt-Rink, D. S. Chemla, and D. A. B. Miller, Phys. Rev. B **32**, 6601 (1985).
[16]W. H. Knox, C. Hirlimann, D. A. B. Miller, J. Shah, D. S. Chemla, and C. V. Shank, Phys. Rev. Lett. **56**, 1191 (1986).
[17]J. S. Blakemore, J. Appl. Phys. **53**, 123 (1982).
[18]For a review, see J. P. Wolfe, J. Lumin. **30**, 82 (1985).
[19]N. N. Zinov'ev, L. P. Ivanov, V. I. Kozub, and I. D. Yaroshetshii, Zh. Eksp. Teor. Fiz. **84**, 1761 (1983) [Sov. Phys.—JETP **57**, 1027 (1983)].
[20]M. Greenstein and J. P. Wolfe, Phys. Rev. Lett. **41**, 715 (1978).
[21]K. Hess, *Advanced Theory of Semiconductor Devices* (Prentice-Hall, Englewood Cliffs, 1988).
[22]R. O. Carlson, G. A. Slack, and S. J. Silverman, J. Appl. Phys. **36**, 505 (1965).
[23]T. C. Cetas, C. R. Tilford, and C. A. Swenson, Phys. Rev. **174**, 835 (1968).
[24]F. O. Müller and R. Zimmerman, in *Physics of Semiconductors, Proceedings of the Fourteenth International Conference on the Physics of Semiconductors, Edinburgh, 1978,* edited by B. L. H. Wilson (Institute of Physics, London, 1979), p. 165.
[25]J. C. Hensel and R. C. Dynes, Phys. Rev. Lett. **39**, 969 (1977).
[26]L. V. Keldysh, Pis'ma Zh. Eksp. Teor. Fiz. **23**, 100 (1976) [JETP Lett. **23**, 86 (1976)]. V. S. Bagaev, L. V. Keldysh, N. N. Sibeldin and B. A. Tsvetkov, Zh. Eksp. Teor. Fiz. **70**, 702 (1976) [Sov. Phys.—JETP **43**, 362 (1976)].
[27]M. Greenstein, M. A. Tamor, and J. P. Wolfe, Phys. Rev. B **26**, 5604 (1982).
[28]H. M. van Driel, J. S. Preston, and M. I. Gallant, Appl. Phys. Lett. **40**, 385 (1982).
[29]D. J. Ershine, A. J. Taylor, and C. L. Tang, Appl. Phys. Lett. **45**, 54 (1984).
[30]D. V. Kazakovtsev and I. B. Levinson, Zh. Eksp. Teor. Fiz. **88**, 2228 (1985) [Sov. Phys.—JETP **61**, 1318 (1985)].